Energy Proceedings
Vol 29, 2022
ISSN 2004-2965

A thermoacoustic refrigerator with a compact thermal buffer tube[#]

Tze Yeung Cho[14], Jingyuan Xu[12*], Ercang Luo[3], Simone Hochgreb[1]

[1]Department of Engineering, University of Cambridge, Cambridge CB2 1PZ, England
[2]Mechanical and Electrical Engineering Division, Karlsruhe Institute of Technology, Karlsruhe 76344, Germany
[3]CAS Key Laboratoury of Cryogenics, TIPC, Chinese Academy of Sciences, Beijing 100190, China
[4]Gonville & Caius College, Cambridge CB2 1TA, England
[*]Corresponding author. E-mail address: jingyuan.xu@kit.edu.

ABSTRACT

The development of thermoacoustic refrigeration technology has been held back by low power density and high required temperatures. The present work proposes and simulates a compact, multi-stage loop thermoacoustic refrigeration system with integrated stages connected by a short thermal buffer tube at the heating-cooling section interface. This arrangement improves power density and reduces friction losses. Designed to operate at a cooling temperature between 200 and 290 K, and powered by low-grade heat input at around 450 to 600 K at 2.0 MPa mean pressure and 293 K ambient temperature, the system can achieve relatively high power density and low onset temperature. Simulation results show a four-stage system can produce a maximum cooling power output of around 5 to 10 kW with an overall axial length of less than 12 m. The system also requires a low onset temperature difference at approximately 35 K between heat input and ambient for the system to sustain limit cycle oscillations.

Keywords: thermoacoustic, refrigeration, engine, waste heat, compact

NOMENCLATURE

Abbreviations	
COP	Coefficient of performance
(for thermoacoustic components)	
AHXc	Ambient heat exchanger of cooler
AHXe	Ambient heat exchanger of engine
CHX	Cold heat exchanger
HHX	Hot heat exchanger
HX	Heat exchanger
PT	Pulse tube
REGc	Regenerator of cooler
REGe	Regenerator of engine
RT	Resonance tube
sAHX	Secondary ambient heat exchanger
TBT	Thermal buffer tube

Symbols	
Latin	
d_{hyd}	Hydraulic diameter
d_{wir}	Wire diameter
k	Thermal conductivity
l	Length
$\mathbf{M}$	Transfer matrix
$\overline{P}$	Mean pressure
p	Pressure
Q	Thermal power
T	Temperature
t	Time
U	Volumetric flow rate
u	Velocity
W	Mechanical work
X	Exergy
Greek	
η	Efficiency
ν	Kinematic viscosity
π_{wal}	Wall thickenss
ρ	Density
ϕ	Phase
ϕ_{por}	Porosity
ψ	Fluid property (equation 1)
Subscripts	
$\overline{\circ}$	Time mean value of $\circ$
1	Primary mode
aut	Auto-
c	Cool
cmp	Component
h	Hot
in	Inlet (towards engine end)
ons	Onset
out	Outlet (towards cooler end)
r	Radial direction
stg	Stage

This is a paper for the 14th International Conference on Applied Energy - ICAE2022, Aug. 8-11, 2022, Bochum, Germany.

1. INTRODUCTION

Global demand for refrigeration devices is growing at a rate of 3% per year [1]. Refrigeration in the residential sector in Japan, Korea, and the USA accounts over 14% share of electricity consumption [2], and nearly 7% of electricity worldwide in 2016, primarily for space cooling [3]. Global cooling-related CO_2 emissions tripled between 1990 and 2016, reaching around 1135 Mt, which accounts for over 10% of the global power generation sector CO_2 [3].

Thermoacoustic refrigeration is a possible alternative cooling method [4]. The system works by conversion of thermal energy into acoustic work, which then drives a heat pump without any moving components. In particular, travelling-wave thermoacoustic refrigerators have been shown to offer higher achievable efficiency in a significant breakthrough [5]. A number of alternative similar designs have been suggested thereafter, including multi-stage-loop systems with smaller dimensions [6], higher energy density [7], and improved exergy efficiency [8, 9]. However, they all achieved relatively low power density, where a large amount of space is taken by resonance tubes.

Previous designs of self-driven thermoacoustic cooling systems [5, 6, 8, 9] position engine and cooler in separated stages. They are connected either as branches of the main loop, or stages coupled by long resonance tubes. This arrangement enables the phase shifting of the pressure vs. flow rate of the working fluid to achieve maximum acoustic power conversion. The connecting resonance tubes between heater and cooler can be long and therefore diminish power density, and increase viscous losses. Their decreased diameter alters the acoustic impedance and introduces losses due to jet-driven streaming at the boundaries.

The present work proposes a thermoacoustic refrigeration system with the heating (engine) and cooling (refrigeration) sections constructed as two segments in a unified stage. Instead of a resonance tube, a thermal buffer tube with the same diameter as the adjacent components is used to provide the necessary impedance between engine and cooler sections. This design improves the power density by reducing the overall axial length of the system, and increasing efficiency by minimising losses caused by resonance tubes.

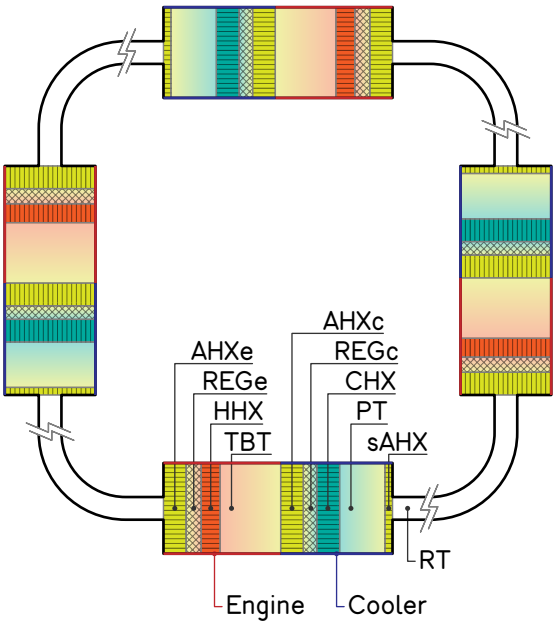

Figure 1: Physical arrangement of a four-stage thermoacoustic refrigerator. The two-dimensional sketches of thermoacoustic cores are drawn to-scale, but not the resonance tubes.

2. SYSTEM CONFIGURATION

Figure 1 illustrates a four-stage variant of a multi-stage loop design. In an integrated heating-cooling stage, the engine section consists of high and ambient temperature

Unit	Component	Diameter [mm]	Length [mm]	Other dimensions
Engine	AHXe	120	30	Shell-tube type, $\phi_{por} = 20\%$, $d_{hyd} = 1\,\mathrm{mm}$
	REGe		20	Wire mesh stack, $\phi_{por} = 90\%$, $d_{wir} = 38\,\mu\mathrm{m}$
	HHX		25	Shell-tube type, $\phi_{por} = 20\%$, $d_{hyd} = 1\,\mathrm{mm}$
	TBT		70	Thick-wall tube $\pi_{wal} = 5\,\mathrm{mm}$
Cooler	AHXc		30	Shell-tube type, $\phi_{por} = 20\%$, $d_{hyd} = 1\,\mathrm{mm}$
	REGc		18	Wire mesh stack, $\phi_{por} = 90\%$, $d_{wir} = 20\,\mu\mathrm{m}$
	CHX		30	Shell-tube type, $\phi_{por} = 20\%$, $d_{hyd} = 1\,\mathrm{mm}$
	PT		60	Thick-wall tube $\pi_{wal} = 2.2\,\mathrm{mm}$
	sAHX		10	Shell-tube type, $\phi_{por} = 20\%$, $d_{hyd} = 1\,\mathrm{mm}$

Table 1: Dimensions of each component in the thermoacoustic system.

Number of stages	Diameter [mm]	Length [mm]
3	32	4360
4	28	2770
5	30	2100
6	31	1670

Table 2: Optimum dimensions of resonance tubes using different numbers of stages.

heat exchangers (HHX, AHXe) connected by a regenerator (REGe), and the cooling section consisting of an ambient and cold end heat exchangers (CHX, AHXc) connected by a second regenerator (REGc). A thermal buffer tube (TBT) connects the engine and cooler sections, and a secondary ambient temperature is connected to the CHX via a pulse tube (PT) to diminish the unwanted thermal loss. A final resonance (or compliance) tube (RT) is required to couple two integrated stages by establishing a correct phase of a travelling wave. Therefore, by altering the geometry of core sections, a usually long RT between engine outlet and cooler inlet is made unnecessary and replaced by the TBT, and one RT remains per stage to ensure the inertia of the resonating fluid. This improved design results in a higher power density compared to conventional systems. The design fits a working cooling temperature range of cooling between 200 and 290 K, heating at a maximum of 600 K, ambient temperature at 293 K, and mean operating pressure at 2.0 MPa. All cores have identical dimensions regardless of the number of stages, whereas RTs have different dimensions for different number of stages to optimise the acoustic field in cores, as listed in Table 1. Dimensions of the RT between engine-cooling core for all systems are listed in Table 2.

3. SIMULATION AND ANALYSIS

3.1 Network modelling

We used DELTAEC [10] acoustic network analysis tool to simulate the cycles and predict the performance of the device. The code solves the linearised, periodic governing equations by assuming all oscillations are sinusoidal and at their primary resonance [11, 4], so that each scalar property ψ can be represented as:

$$\psi(x,t) = \overline{\psi} + \psi_1 e^{i(\omega t - \phi_\psi(x))}, \tag{1}$$

and ϕ is a location-dependent phase.

It solves the one-dimensionalised perturbed equations in the frequency domain. Equations for mass (2), momentum (3), and energy (4) described in Rott's theory [11, 4] are applied, as follows.

$$i\omega\rho_1 = -\overline{\rho}\left(\frac{\partial u_1}{\partial x} + \frac{1}{r}\frac{\partial r u_{r1}}{\partial r}\right), \tag{2}$$

$$i\omega u_1 = -\frac{1}{\overline{\rho}}\frac{\mathrm{d}p_1}{\mathrm{d}x} + \frac{\nu}{r}\frac{\partial}{\partial r}\left(r\frac{\partial u_1}{\partial r}\right), \tag{3}$$

$$i\omega\overline{\rho}c_p T_1 + \overline{\rho}c_p\frac{\mathrm{d}\overline{T}}{\mathrm{d}x}u_1 = i\omega p_1 + \frac{k}{r}\frac{\partial}{\partial r}\left(r\frac{\partial T_1}{\partial r}\right), \tag{4}$$

where the (ψ_1) subscript indicates the perturbed, as opposed to the mean ($\overline{\psi}$), quantity, and the radial components are eliminated outside heat exchangers, where the approximated solid to working fluid heat transfer are evaluated locally.

3.2 Phase of acoustic field

The multi-stage looped model can be simplified into a single-stage section, as the circular character implies that in a system with n stages, the phase shift at two arbitrary points at a distance of one-stage apart (m^{th} and $(m+1)^{\text{th}}$ stage) corresponds to a auto-phase difference,

$$\phi_{\psi,\text{aut}} = \phi_{\psi,x,(m+1)} - \phi_{\psi,x,m} = -\frac{2\pi}{n}. \tag{5}$$

Furthermore, each variable is phased differently as each component has a distinct impedance. The phase difference between pressure and flow rate, ϕ_{pU}, is important for the performance of the system, and defined as,

$$\begin{aligned} p &= \overline{P} + p_1 e^{i(\omega t - \phi_p)}; \\ U &= U_1 e^{i(\omega t - \phi_U)}; \\ \phi_{pU} &= \phi_p - \phi_U. \end{aligned} \tag{6}$$

3.3 Onset analysis

We apply a *transfer matrix* method for calculating the onset conditions based on the same equations used in analytical solutions of the linearised periodic equations [4] and by DELTAEC [10]. This method has been applied and validated in previous research such as in ref. [12, 13, 14]. In the analysis, Eqs. 2 and 3, can be simplified to a matrix form,

$$\frac{\mathrm{d}}{\mathrm{d}x}\begin{pmatrix} p_1 \\ u_1 \end{pmatrix} = \mathbf{Z}_{\mathrm{d}x}\begin{pmatrix} p_1 \\ u_1 \end{pmatrix}, \tag{7}$$

and by integration in x across a component,

$$\begin{pmatrix} p_1 \\ u_1 \end{pmatrix}_{\text{out}} = \mathbf{M}_{\text{cmp}}\begin{pmatrix} p_1 \\ u_1 \end{pmatrix}_{\text{in}}, \tag{8}$$

where $\mathbf{M}_{\text{cmp}}$ is the *transfer matrix* for the component evaluated. Each component has its own transfer matrix, and the system can be evaluated by linear reversed multiplication of the matrix of each component, as further discussed in Ref. [12].

Each stage in the system is identical, and the same global transfer matrix is applied. Therefore, the values at each location on adjacent stages are connected via the auto-phase difference, ϕ_{aut}, and the calculation can be simplified as,

$$\mathbf{M}_{\text{stg}} \begin{pmatrix} p_1 \\ u_1 \end{pmatrix}_{\text{in}} = \begin{pmatrix} e^{i\phi_{\text{aut}}} & 0 \\ 0 & e^{i\phi_{\text{aut}}} \end{pmatrix} \begin{pmatrix} p_1 \\ u_1 \end{pmatrix}_{\text{in}}. \tag{9}$$

One can evaluate the onset condition for the limit cycle by imposing the boundary conditions to the matrix. All ambient and cold HXs are assumed to be at ambient temperature, and HHXs are at the set operating temperature. The onset condition is satisfied when the determinant of transfer matrix is zero,

$$\det \left[\mathbf{M}_{\text{stg}} - \begin{pmatrix} e^{i\phi_{\text{aut}}} & 0 \\ 0 & e^{i\phi_{\text{aut}}} \end{pmatrix} \right] = 0. \tag{10}$$

3.4 *Efficiency*

The thermal efficiency, η_Q, is defined as the ratio of output cooling energy rate to the input heating energy rate. This is not to be confused with the usual coefficient of performance (COP) used in vapour-compression refrigeration, which is the ratio of cooling output to work input rate. An exergy efficiency, η_X, can also be defined to account for the highest achievable efficiency (Carnot) for the given heating and cooling temperatures.

For a system generating thermal output Q_{out} at T_{out} with thermal input Q_{in} at T_{in} under ambient temperature at T_0,

$$\eta_Q = \frac{Q_{\text{c}}}{Q_{\text{h}}} \tag{11}$$

$$\eta_X = \eta_Q \left| \frac{T_{\text{h}}}{T_{\text{c}}} \frac{T_{\text{c}} - T_0}{T_{\text{h}} - T_0} \right|. \tag{12}$$

4. RESULTS AND DISCUSSION

4.1 *Dimensions of thermal buffer tube*

The dimensions in Table 1 were defined by iterative optimisations. We positioned a short TBT between engine and cooler sections to adjust the phase ϕ_{pU}. The length of TBT was designed to optimise thermal efficiency, which usually corresponds to a minimal coupled phase difference $\Delta\phi_{pU}$ in the engine and cooler regenerators. Figure 2 illustrates the optimal length of TBT at different combinations of working temperatures. When the TBT length l_{TBT} is 70 mm, the efficiency hovers around an optimum for the working condition. Figure 3 shows the change in thermal efficiency η_Q and cooling flow Q_{c} as a function of the length of TBT between 60 and 80 mm. Both thermal efficiency and cooling output vary less than 10% when TBT deviates ± 10 mm off its optimal point.

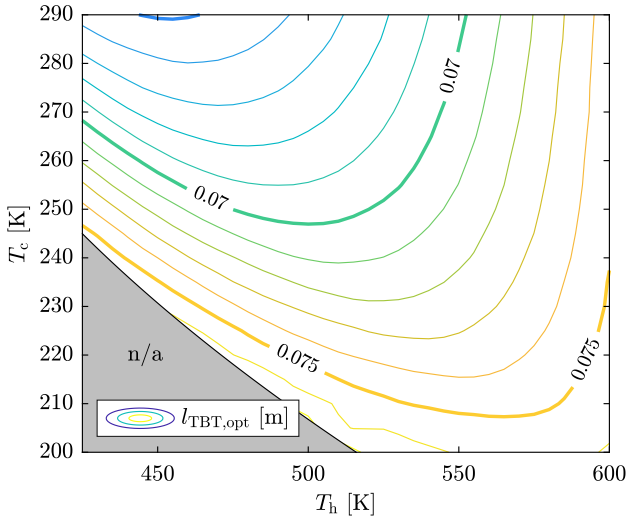

Figure 2: Optimal length of TBT $l_{\text{TBT,opt}}$ for efficiency at temperature combinations with mean pressure at 2.0 MPa and ambient temperature at 293 K.

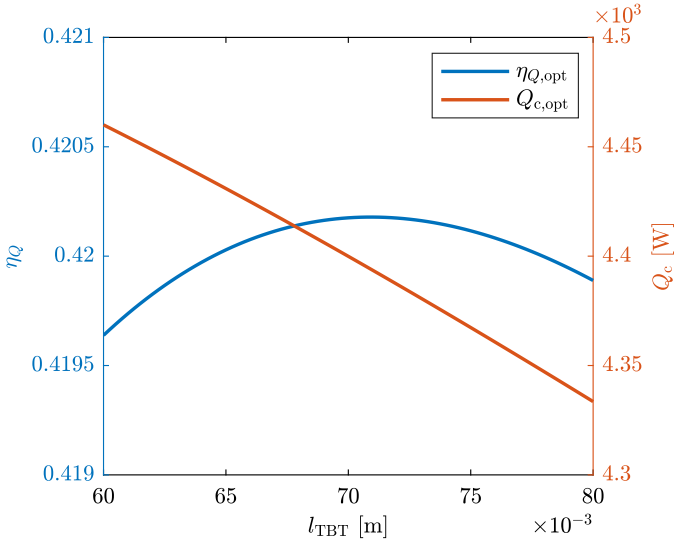

Figure 3: Thermal efficiency η_Q and cooling flow Q_{c} at different TBT length l_{TBT} while HHX at 500 K and CHX at 240 K with mean pressure at 2.0 MPa and ambient temperature at 293 K.

4.2 *Onset characteristics analysis*

The onset conditions are determined using the *transfer matrix* method, as the network modelling tool.Onset corresponds to the minimum temperature required for the working fluid in the system to sustain an acoustic resonance and the respective frequency. Figure 4 shows the onset temperature and frequency for different mean pressures of the devices with 3 to 6 stages. Onset temperatures (Figure 4a) decrease from about 80-100 K at the lowest pressure tested to 20 K for the highest pressure of 3.5 MPa, mainly as a result of the effect of density differences at different pressure. Variation between num-

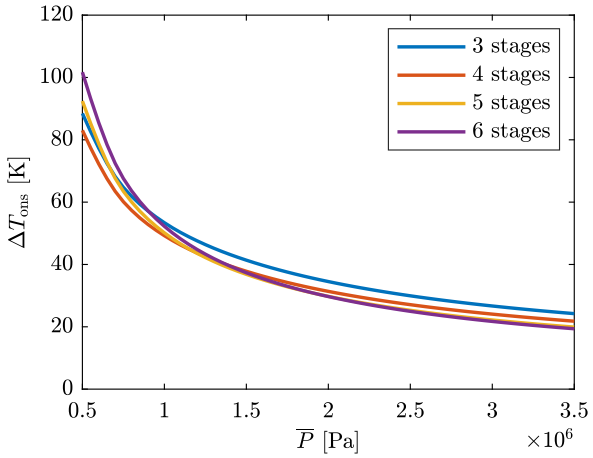

(a) Onset temperature difference.

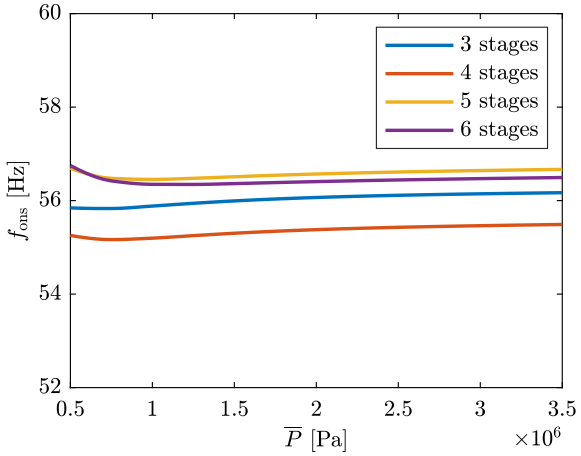

(b) Onset frequency.

Figure 4: Variation of onset frequency and temperature difference of system with different stages at various mean pressures.

ber of stages is small, as the cores are designed to operate under similar conditions. Onset frequency (Figure 4b) changes little under varying pressure, as this result depends primarily on geometry.

4.3 Steady state performance

The system cooling output Q_c is shown in Figure 5a for a range of temperature settings. Cooling output increases relatively linearly with either heating temperature T_h or cooling temperature T_c, as thermal input increases as T_h increases and lower thermal potential is required when T_c increases.

This cooling output corresponds to the thermal efficiency η_Q and exergy efficiency η_X plotted as contours in Figures 5b and 5c. Thermal efficiency increases as the cooling temperature increases, whereas it increases to a maximum and decreases thereafter while the heating temperature is increased. An efficiency of over 0.6 is

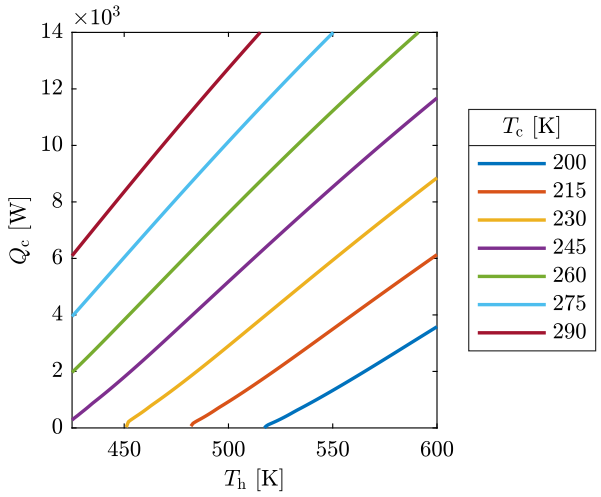

(a) Cooling power at different temperature conditions.

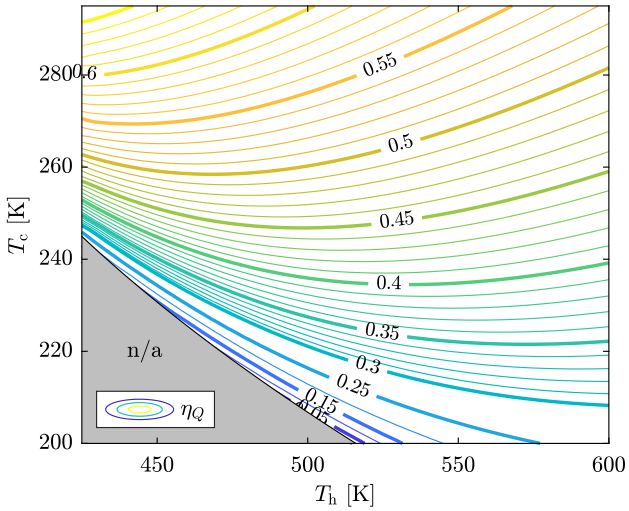

(b) Thermal efficiency η_Q at different temperature conditions ranging between 0.20 and 0.65.

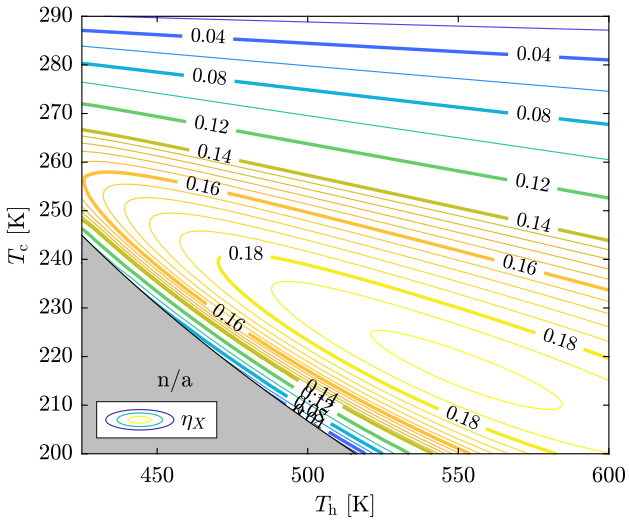

(c) Exergy efficiency η_X at different temperature conditions ranging between 0.10 and 0.20.

Figure 5: Simulation results of cooling power and efficiency generated by DELTAEC with mean pressure at 2 MPa and ambient temperature 293 K.

achieved when cooling temperature is above 280 K. The simulated exergy efficiency achieves a maximum of 0.189 when heated to 550 K and producing cooling at 220 K.

5. CONCLUSIONS

Previous designs of thermoacoustic refrigeration systems have heating and cooling segments designed as stages separated by long resonance tubes, which reduces power density, increases complexity, and incurring losses. A design of thermoacoustic refrigerator with the compact integrated heating-cooling stages, operating at cooling temperature between 200 and 290 K with low-grade heat input at around 450 to 600 K, 2.0 MPa mean pressure, and 293 K ambient temperature is proposed and analysed in this article. Using a network modelling method and analytical simulations, we found that for a four-stage system at 2.0 MPa mean pressure and 293 K ambient temperature,

- overall axial length of one stage in a four-stage system is approximately 3 m, with the core section less than 0.3 m;
- highest efficiency is achieved using TBTs with a length of 70 mm;
- the system onsets at approximately 35 K temperature difference between hot and ambient, and oscillates in a limit cycle at 55 Hz resonance frequency - this makes it a feasible candidate for operation with solar power;
- the refrigeration system is expected to produce maximum power around 5 to 10 kW depending on input and output temperature conditions;
- maximum thermal efficiency over 0.6 and exergy efficiency of 0.189 is achieved by the system.

ACKNOWLEDGEMENT

T.Y. Cho would like to express gratitude for all the help, especially the insightful discussions and proof-reading from friends and colleagues, received during this project.

REFERENCE

[1] IEA. Cooling - Fuels & Technologies. 2020. Available from: https : / / www . iea . org / fuels - and - technologies/cooling [Accessed on: 2021 Jul 31]

[2] Choi S, Han U, Cho H, Lee H. Review: Recent advances in household refrigerator cycle technologies. Applied Thermal Engineering 2018; 132:560–74

[3] OECD/IEA. The Future of Cooling. 2018. Available from: https://www.iea.org/reports/the-future-of-cooling [Accessed on: 2022 Jun 27]

[4] Swift GW. Thermoacoustics: A Unifying perspective for some engines and refrigerators: Second edition. Cham: Springer International Publishing; 2017

[5] De Blok K. Novel 4-Stage Traveling Wave Thermoacoustic Power Generator. *ASME 2010 3rd Joint US-European Fluids Engineering Summer Meeting*. Montreal, Canada: ASMEDC; 2010:FEDSM–ICNMM2010–30527

[6] Hotta K, Sakamoto Si, Tsukamoto D, Watanabe Y. Miniaturization of the Loop-Tube-Type Thermoacoustic Cooling System: Effect of the Installation Position of Heat Pump and Working Gas in the Tube. Japanese Journal of Applied Physics 2010; 49:07HE17

[7] Zhao Y, Yang Z, Luo E, Zhou Y. Travelling-wave thermoacoustic high-temperature heat pump for industrial waste heat recovery. Energy 2014; 77:397–402

[8] Xu J, Zhang L, Hu J, Wu Z, Bi T, Dai W, Luo E. An efficient looped multiple-stage thermoacoustically-driven cryocooler for liquefaction and recondensation of natural gas. Energy 2016; 101:427–33

[9] Xu J, Yu G, Zhang L, Dai W, Luo E. Theoretical analysis of two coupling modes of a 300-Hz three-stage thermoacoustically driven cryocooler system at liquid nitrogen temperature range. Applied Energy 2017; 185:2134–41

[10] Clark JP, Ward WC, Swift GW. Design environment for low-amplitude thermoacoustic energy conversion (DeltaEC). 2007

[11] Rott N. Damped and thermally driven acoustic oscillations in wide and narrow tubes. Zeitschrift für angewandte Mathematik und Physik ZAMP 1969; 20:230–43

[12] Xu J, Luo E, Hochgreb S. Study on a heat-driven thermoacoustic refrigerator for low-grade heat recovery. Applied Energy 2020; 271:115167

[13] Chi J, Xu J, Zhang L, Wu Z, Hu J, Luo E. Study of a gas-liquid-coupled heat-driven room-temperature thermoacoustic refrigerator with different working gases. Energy Conversion and Management 2021; 246:114657

[14] Bahrami M, Ommi F. Developing an augmented onset model for a thermoacoustically-driven, pulse tube cryocooler. Sustainable Energy Technologies and Assessments 2021; 47:101402